



ARL-TR-8080 • Aug 2017



Evaluation of a Belt-Cast Austenitic Steel Alloy from Salzgitter Mannesmann Forschung: Effect of Hardness on the Ballistic Resistance against Two 0.30-cal. Projectile Types

**by Laszlo J Kecskes, Xiaoxue Chen, Jianguo Li, Vincent H
Hammond, Qiuming Wei, and Tyrone L Jones**

NOTICES

Disclaimers

The findings in this report are not to be construed as an official Department of the Army position unless so designated by other authorized documents.

Citation of manufacturer's or trade names does not constitute an official endorsement or approval of the use thereof.

Destroy this report when it is no longer needed. Do not return it to the originator.



Evaluation of a Belt-Cast Austenitic Steel Alloy from Salzgitter Mannesmann Forschung: Effect of Hardness on the Ballistic Resistance against Two 0.30-cal. Projectile Types

by Laszlo J Kecskes, Vincent H Hammond, and Tyrone L Jones
Weapons and Materials Research Directorate, ARL

Xiaoxue Chen, Jianguo Li, and Qiuming Wei
University of North Carolina, Charlotte, North Carolina

REPORT DOCUMENTATION PAGE				Form Approved OMB No. 0704-0188	
<p>Public reporting burden for this collection of information is estimated to average 1 hour per response, including the time for reviewing instructions, searching existing data sources, gathering and maintaining the data needed, and completing and reviewing the collection information. Send comments regarding this burden estimate or any other aspect of this collection of information, including suggestions for reducing the burden, to Department of Defense, Washington Headquarters Services, Directorate for Information Operations and Reports (0704-0188), 1215 Jefferson Davis Highway, Suite 1204, Arlington, VA 22202-4302. Respondents should be aware that notwithstanding any other provision of law, no person shall be subject to any penalty for failing to comply with a collection of information if it does not display a currently valid OMB control number.</p> <p>PLEASE DO NOT RETURN YOUR FORM TO THE ABOVE ADDRESS.</p>					
1. REPORT DATE (DD-MM-YYYY) August 2017		2. REPORT TYPE Technical Report		3. DATES COVERED (From - To)	
4. TITLE AND SUBTITLE Evaluation of a Belt-Cast Austenitic Steel Alloy from Salzgitter Mannesmann Forschung; Effect of Hardness on the Ballistic Resistance against Two 0.30-cal. Projectile Types				5a. CONTRACT NUMBER	
				5b. GRANT NUMBER	
				5c. PROGRAM ELEMENT NUMBER	
6. AUTHOR(S) Laszlo J Kecskes, Xiaoxue Chen, Jianguo Li, Vincent H Hammond, Qiuming Wei, and Tyrone L Jones				5d. PROJECT NUMBER	
				5e. TASK NUMBER	
				5f. WORK UNIT NUMBER	
7. PERFORMING ORGANIZATION NAME(S) AND ADDRESS(ES) US Army Research Laboratory ATTN: RDRL-WMP-A Aberdeen Proving Ground, MD 21005-5069				8. PERFORMING ORGANIZATION REPORT NUMBER ARL-TR-8080	
9. SPONSORING/MONITORING AGENCY NAME(S) AND ADDRESS(ES)				10. SPONSOR/MONITOR'S ACRONYM(S)	
				11. SPONSOR/MONITOR'S REPORT NUMBER(S)	
12. DISTRIBUTION/AVAILABILITY STATEMENT Approved for public release; distribution is unlimited.					
13. SUPPLEMENTARY NOTES					
14. ABSTRACT Representative samples of 5-mm thick, belt-cast, high-manganese austenitic steel were obtained from Salzgitter Mannesmann Forschung, a German steel manufacturing concern. The steel samples were subjected to microstructural and quasi- and high-strain-rate mechanical property characterizations. Additionally, the steel was comparatively evaluated ballistically against 2 types of threats, namely, a 0.30-cal. M2 ball projectile and a fragment-simulating projectile. The evaluation showed that overall, an equivalent thickness rolled homogeneous armor plate performed better than the German steel.					
15. SUBJECT TERMS austenitic steel, Salzgitter, microstructural properties, ballistic testing, ball projectile, fragment-simulating projectile					
16. SECURITY CLASSIFICATION OF:			17. LIMITATION OF ABSTRACT UU	18. NUMBER OF PAGES 40	19a. NAME OF RESPONSIBLE PERSON Laszlo J Kecskes
a. REPORT Unclassified	b. ABSTRACT Unclassified	c. THIS PAGE Unclassified			19b. TELEPHONE NUMBER (Include area code) 410-306-0811

Contents

List of Figures	iv
List of Tables	v
1. Introduction	1
2. Background	3
3. Experimental Procedures	4
4. Results and Discussion	7
4.1 Microstructural and Mechanical Properties	7
4.2 Ballistic Testing	14
5. Summary and Conclusions	22
6. References	23
Appendix. Ballistic Test Data	25
List of Symbols, Abbreviations, and Acronyms	31
Distribution List	32

List of Figures

Fig. 1	Comparison of the mechanical properties of conventional and advanced body-centered cubic (BCC) lattice-based steels with face-centered cubic (FCC) lattice-based chromium-nickel (Cr-Ni) (AUST SS) and high-Mn (TWIP, TRIP, and TRIPLEX) austenitic steels. Reprinted with permission.	2
Fig. 2	Experimental setup. A schematic diagram of the Split-Hopkinson (Kolsky) pressure bar.	6
Fig. 3	Optical micrographs of the as-received SecoSal300 Salzgitter steel: a) a lower magnification image revealing the uniformity of the microstructure and b) a higher magnification image showing that the average grain size is roughly 5–10 μm	7
Fig. 4	TEM micrographs of the as-received SecoSal300 Salzgitter steel: a) typical grain microstructure, b) the grain interior with dislocations, c) a stacking fault, and d) a selected area diffraction pattern (SADP) revealing the FCC crystal structure.....	8
Fig. 5	XRD scan of the SecoSal300 steel. The data reveal the Bragg peaks due to γ -Fe only. The scans were plotted on a logarithmic scale and the individual scans were offset for clarity.	9
Fig. 6	Quasi-static true stress-true strain curves for the SecoSal300 Salzgitter steel: a) tension and b) compression data for all orientations relative to the rolling direction. Despite the rolling, the response of the material is isotropic.....	10
Fig. 7	Dynamic compressive true stress-true strain curves for the SecoSal300 Salzgitter steel: a) response at 3500 s^{-1} and b) response at 6000 s^{-1} . Both these data and a comparison with the quasi-static compression data show that the material has a very strong strain-hardening response. Again, note the isotropy of the material.....	11
Fig. 8	Postmortem SEM of the dynamic compression samples, tested at 6000 s^{-1} . Images show a) macro and b) microscale views of the specimen loaded in the transverse direction and c) macro- and d) microscale views of the specimen loaded in the rolling direction.	12
Fig. 9	TEM micrographs of the SecoSal300 Salzgitter steel after tension testing: a) typical BF image with nanoscale twins, b) corresponding SADP, c) another region showing the presence of twins, and d) corresponding SADP. Note the double diffraction spots in the SADPs are attributed to twinning.	13
Fig. 10	Tensile test specimens after failure, rolling direction a) and transverse b) direction, respectively.	13
Fig. 11	SEM of the fracture surface at increasing magnifications. Composite image in a), and higher magnifications revealing the ductile nature of the failure in b) and c), respectively.....	14

Fig. 12	Schematic of the 0.30-cal. M2 ball projectile	15
Fig. 13	Schematic of the 0.30-cal. FSP	15
Fig. 14	Postballistic front and back side photographs of the 5.004-mm Salzgitter steel plate vs. the 0.30-cal. M2 ball projectile. Note the bulging of the back face for the penetrators that did not perforate the plate.....	17
Fig. 15	Postballistic front and back side photographs of the 4.947-mm RHA plate vs. the 0.30-cal. M2 ball projectile. Note the lack of bulging for the penetrators that did not perforate the plate.....	18
Fig. 16	Postballistic front and back side photographs of the 5.004-mm Salzgitter steel plate vs. the 0.30-cal. FSP	19
Fig. 17	Postballistic front and back side photographs of the 4.947-mm RHA plate vs. the 0.30-cal. FSP.....	20

List of Tables

Table 1	Salzgitter steel: chemical analysis results	5
Table 2	Ballistic results of the RHA and Salzgitter steel plates vs. the 0.30-cal. M2 ball projectile and the 0.30-cal. FSP.....	16

INTENTIONALLY LEFT BLANK.

1. Introduction

Since the original discovery on the benefits of manganese (Mn) and carbon (C) additions in steels by Hadfield and Burnham,¹ there has been a continuous development of steels with high Mn and high aluminum (Al) contents. The original iron (Fe)-Mn-C Hadfield steels with 10–14 wt% Mn and 1.0–1.4 wt% C had very high work-hardening rates, yield strengths of approximately 380 MPa, and ultimate tensile strengths of about approximately 970 MPa.² The roles of the Mn and C were to stabilize the high-temperature austenite phase to ambient temperatures. As illustrated in Fig. 1, the special subclasses of multiphase, high-strength steels (i.e., twinning-induced plasticity [TWIP], transformation-induced plasticity [TRIP], and TRIPLEX) are fully austenitic and have extremely high ductility and ultimate tensile strengths. Typically, in TWIP and TRIP steels, addition of other alloying elements such as Al and silicon (Si) are to alter the stacking fault energy (SFE), accelerate ferrite-bainite formation, and limit the formation of carbide (cementite). Although, it is primarily the C content that determines the SFE and, thus, the TWIP or TRIP mechanism. In contrast, TRIPLEX steels are usually based on much higher Mn and Al contents, consisting of Fe-Mn-C-Al, wherein the relationship between the components of austenite, ferrite, and κ -carbides determines the mechanical and microstructural properties.

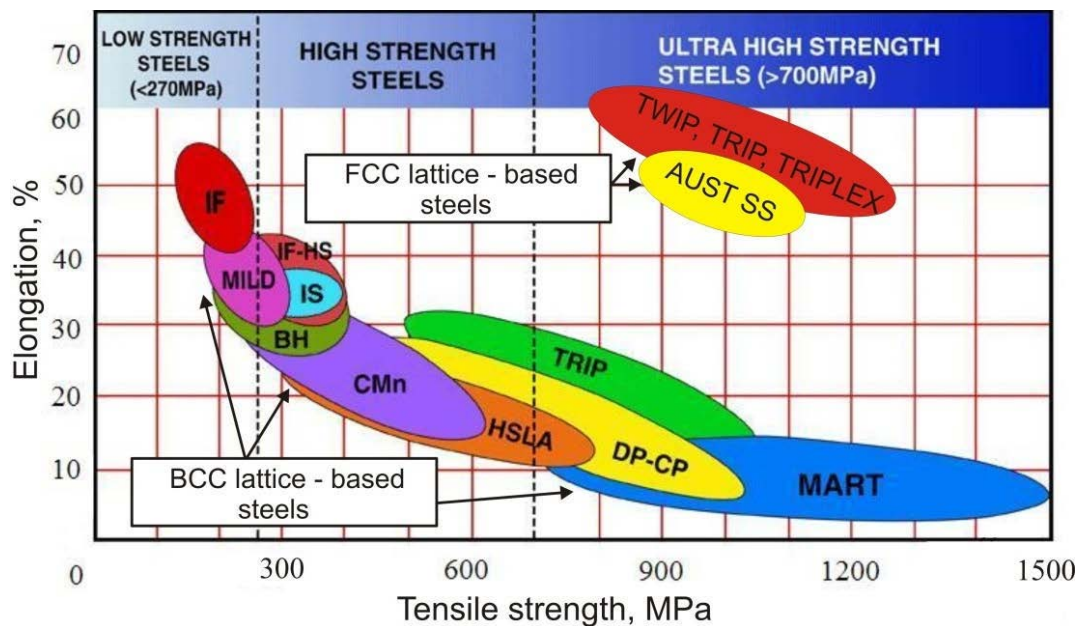


Fig. 1 Comparison of the mechanical properties of conventional and advanced body-centered cubic (BCC) lattice-based steels with face-centered cubic (FCC) lattice-based chromium-nickel (Cr-Ni) (AUST SS) and high-Mn (TWIP, TRIP, and TRIPLEX) austenitic steels. Reprinted with permission. ©2012 Ozgowicz W, Kurc-Lisiecka A, Grajcar A. Published in Chapter 4 of *Environmental and Industrial Corrosion Practical and Theoretical Aspects*, edited by Salas B, Schorr M, December 12, 2012, under CC BY 3.0 license. Available from <http://dx.doi.org/10.5772/53590>.

Among the many large-scale steel manufacturing concerns, Salzgitter AG, headquartered in Salzgitter, Germany, has been actively engaged in developing the required manufacturing technology and requisite alloy compositions for the production of high-strength and high-ductility security steels. Security steels are commonly used in the energy, mining, and transportation sectors.

In 2015, a promotional company brochure was received from Dr Manuel Otto of the research division, Salzgitter Mannesmann Forschung (Salzgitter, heretofore), titled “Alternative Steel Upgrades for High Strain Rate Applications – SecoSal300”. The data in the brochure indicated comparatively better-than-average steel properties. The brochure also highlighted the challenges for continuous casting operations and potential processing solutions to overcome them: the key steps of a unique belt-casting process under development at Salzgitter.

This material, with a high Mn content, is nominally a fully austenitic steel. As such, it was expected that it would have excellent mechanical properties. However, to date, this alloy has been only produced on an experimental prototyping basis at Salzgitter’s Peine, Germany, belt-casting plant. Because of limitations of the

technology and alloy chemistry, the company was still experiencing fabrication issues that prevent the material from being fabricated in thicker sections. Therefore, currently, only 5-mm-thick plates of the material were available.

Because of the proprietary nature of the belt-casting process and the steel not yet being in production, an extended period of negotiations was required to obtain representative samples of this experimental steel from Salzgitter. As a result, 5 square plates, $305 \times 305 \times 5$ mm (12 inches \times 12 inches \times 5 mm), were procured through Universal Steel America, a US subsidiary of the Salzgitter AG Group, with headquarters in Houston, Texas.

Samples were subjected to chemical analysis to verify composition, microstructural analysis to verify morphology and structure, and (quasi-static and high-strain-rate) mechanical testing (tension and compression) to validate the German results released to us. The quasi-static and high-strain-rate compression tests were performed by Prof Qiuming Wei and his students at the University of North Carolina, Charlotte, North Carolina. Additionally, the plates were of suitable dimensions that they could be subjected to comparative ballistic tests against a 0.30-cal. M2 armor-piercing ball projectile and a 0.30-cal. fragment-simulating projectile (FSP), using rolled homogeneous armor (RHA) plate as a baseline reference.

2. Background

RHA, US Department of Defense MIL-A-12560³ under the CLASS 1 specification, has been the standard of combat ground vehicles of the military against a broad spectrum of ballistic threats for many decades. RHA has relatively high strength with good resistance to penetration while minimizing spall formation. This steel is easily machinable, joinable, and fabricated at relatively low cost in existing production facilities.^{4,5}

RHA is a conventional wrought, medium C, deep-hardening steel similar to the AISI 4300 series of steels. The chemical composition varies with the supplier, with a maximum level of C of 0.30% in a plate as thick as 2 inches (limits frangibility), 0.025% phosphorus, and 0.015% sulfur (known embrittling agents). Typical alloying elements are Cr, molybdenum, Ni, and/or Si, and the plate is fabricated via conventional steel production methods. RHA is ballistically superior to cast steels because of the refinement of grain structure that occurs during rolling.⁶ The maximum variation in chemical composition within any heat of RHA was obtained from Table 1 of MIL-A-12560K.³ The minimum mechanical properties of RHA are listed in Table 2 in Han et al.⁷

The US Army Research Laboratory (ARL) has experimentally found that typical high-strength steel targets, although less ductile, perform better against the M2 armor-piercing ball projectile, while targets with less strength and more ductility perform better against the FSP.⁸ (The M2 armor-piercing ball projectile consists of a core with a softer metal jacket.) More specifically, the M2 ball projectile has a narrow diameter with an ogive nose cone. Its method of failure is to penetrate rather than plug through the target. Although both projectiles are the same caliber (i.e., have the same diameter) at the onset of penetration, the initially larger diameter FSP has a bigger cross-sectional area and thus primarily wants to push the target to create a plug on its back surface. The process of plugging corresponds to an adiabatic shear failure of the target.

This study examined the penetration resistance of 5-mm Salzgitter steel plates versus 5-mm conventional RHA plates. The primary objective was to understand how a higher level of ductility could improve the performance of the plate against a broader spectrum of ballistic threats, namely, the 0.30-cal. M2 ball projectile and the 0.30-cal. FSP.

3. Experimental Procedures

Only the nominal composition, consisting of 15 wt% Mn, 2.5 wt% Si, 2.5 wt% Al, and 0.7 wt% C, of the alloy was provided by Salzgitter. Therefore, the composition of the alloy was verified by sending a section of the plate for chemical analysis to Luvak Inc., Boylston, Massachusetts. C and sulfur were detected via combustion infrared detection, ASTM E 1019-11,⁹ hydrogen was detected via inert gas fusion, ASTM E 1447-09,¹⁰ oxygen and nitrogen were detected via inert gas fusion, ASTM E 1091-11,⁹ and all other elements were detected via direct current plasma emission spectroscopy, ASTM E 1097-12.¹¹ A summary of the results are shown in Table 1. The listed concentrations of the elements are provided on a metals basis.

Table 1 Salzgitter steel: chemical analysis results

Element	wt%	at%
Iron	Balance	Balance
Manganese	14.7	14.2
Silicon	2.49	4.72
Aluminum	2.06	4.06
Chromium	0.083	0.085
Copper	0.075	0.063
Nickel	0.046	0.042
Titanium	0.014	0.016
Molybdenum	0.007	0.0039
Niobium	0.0066	0.0038
Cobalt	0.0057	0.0051
Vanadium	0.0045	0.0047
Interstitials		
Carbon	0.636	...
Oxygen	0.0009	...
Nitrogen	0.0006	...
Hydrogen	0.00033	...
Sulfur	<0.001	...

Based on the medium level of Mn and high C contents, respectively, this alloy belongs in the class of TWIP steels. While the Mn and C are both austenite stabilizers, the addition of Al is to delay the onset of fracture during forming operations.¹²

The constituent phases and texture analysis of the Salzgitter steel was examined with a Bruker AXS D8 Discovery X-ray diffractometer system (Bruker Corp., Billerica, MA). Representative postmortem fracture surface samples for scanning electron microscopy (SEM) using a JEOL 6480 scanning electron microscope (JEOL USA, Inc., Peabody, MA) were examined after tension and compression testing. Samples for transmission electron microscopy (TEM), using a JEOL 2100 TEM equipped with a LaB₆ filament, were prepared by mechanical polishing down to a thickness of less than 100 μm , followed by twin-jet electropolishing, with a Lectropol-5 system (Struers, Inc., Cleveland, OH) using a chemical solution of 90% acetic acid (CH_3COOH) and 10% perchloric acid (HClO_4) at 253 K with an applied voltage of 12 V.

For the quasi-static and high-strain-rate compression experiments, small cuboid-shaped samples were cut from the test plates. Three sets of samples were cut using wire electric discharge machining (EDM) in the 3 orthogonal directions (rolling, transverse, and normal) relative to the plate rolling direction.

Additionally, dogbone-shaped tension samples were cut in 2 orthogonal orientations relative to the rolling direction (one in the rolling and one in the transverse orientation). The specimen dimensions were machined with a gauge length of 25 mm, width of 6 mm, and thickness of 5 mm as required by the ATSM E8/E8M¹³ subscale size specifications.

The quasi-static tensile tests were carried out on an Instron 5580 load frame (Instron, Inc., King of Prussia, PA) with a strain rate of 0.001 s^{-1} . A noncontact video extensometer was used to measure the strain of the sample during tensile loading. The quasi-static compressive tests were conducted on the same load frame. For the quasi-static compression tests, the sample dimensions were $2.5 \times 2.5 \times 5.0 \text{ mm}$, with a gauge length of 5.0 mm. The compressive strain of the specimen was derived based on the crosshead displacement of the loading system. The interfaces between the loading surfaces and the platens were lubricated to reduce friction effects. For each orientation, at least 3 samples with the same conditions were tested to ensure the reproducibility of the experimental results.

The dynamic high-strain-rate uniaxial compression tests were conducted using a Split-Hopkinson (Kolsky) pressure bar system (a schematic is shown in Fig. 2). Follansbee¹⁴ and Gray¹⁵ provide a detailed description of the tests and operation, respectively. For the high-strain-rate tests, the sample dimensions were $2.5 \times 2.5 \times 2.0 \text{ mm}$, with a gauge length of 2.0 mm. To minimize friction, the interfaces between the bars and the specimen were carefully lubricated with a multipurpose lithium-based grease. During the tests, strain rates above 1000 s^{-1} were routinely attained.

In each case, the impact or contact surfaces of mechanical property samples were polished to a $6.5\text{-}\mu\text{m}$ (#1200 grit polishing paper) finish to remove the EDM-induced recast surface layer. The side surfaces used for SEM observations were polished to a $0.3\text{-}\mu\text{m}$ finish before the start of the tests.

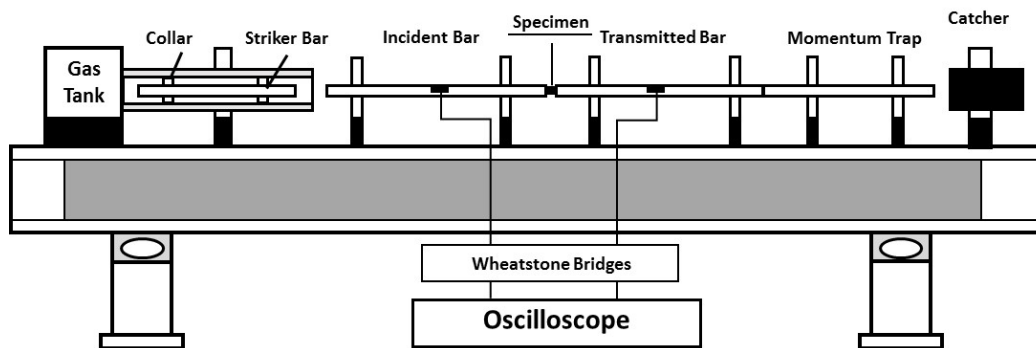


Fig. 2 Experimental setup. A schematic diagram of the Split-Hopkinson (Kolsky) pressure bar.

4. Results and Discussion

4.1 Microstructural and Mechanical Properties

A density of 7.46 g/cm^3 was measured (water immersion) for the alloy and the chemical analysis confirmed the nominal composition. Compared to RHA with a density of 7.8 g/cm^3 , this steel is about 5% less dense.

Optical and TEM analyses of the as-received material revealed a relatively fine grain-size (see Figs. 3 and 4, respectively). The optical micrographs shown in Fig. 3 reveal a mostly uniform microstructure. However, because of the severe rolling deformation imparted to the plate, the grain boundaries were rough and a simple Nital etchant was not effective in bringing out the grain boundary contrast.

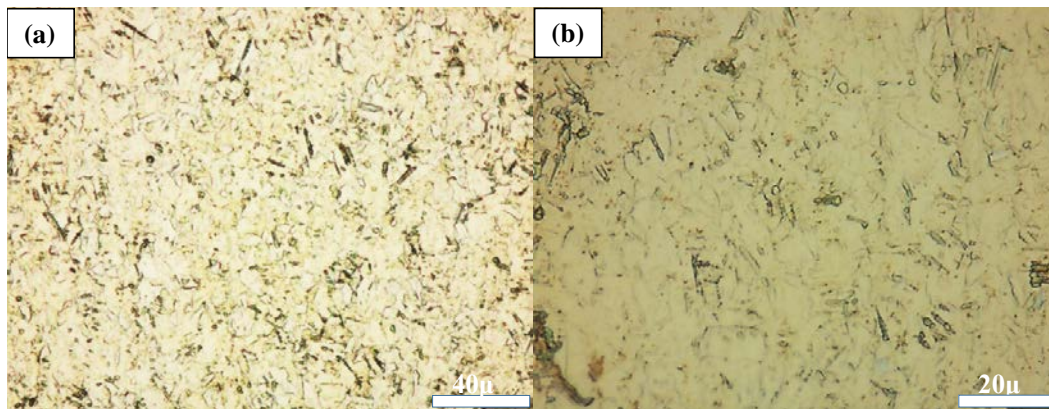


Fig. 3 Optical micrographs of the as-received SecoSal300 Salzgitter steel: a) a lower magnification image revealing the uniformity of the microstructure and b) a higher magnification image showing that the average grain size is roughly $5\text{--}10 \mu\text{m}$

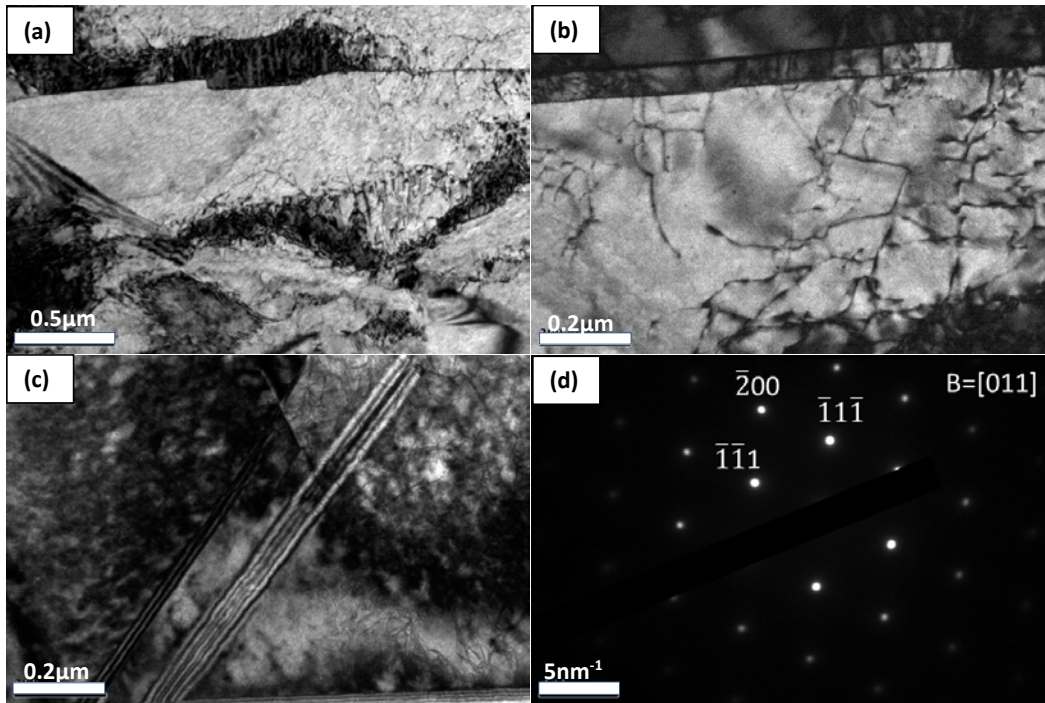


Fig. 4 TEM micrographs of the as-received SecoSal300 Salzgitter steel: a) typical grain microstructure, b) the grain interior with dislocations, c) a stacking fault, and d) a selected area diffraction pattern (SADP) revealing the FCC crystal structure

In Fig. 4a, the bright field (BF) TEM image reveals a fairly clean grain interior, a precipitate along the grain boundary, and dislocations. In Fig. 4b, dislocation networks can be seen more clearly within the grain interior. The dislocations are likely emitted from the grain boundaries and defects. In addition to these features, some of the grains contain stacking faults (Fig. 4c). The SADP shown in Fig. 4d indicates that the material has an FCC crystal structure, thereby confirming that it is fully austenitic. Additionally, as shown in Fig. 5, this fact is also confirmed with X-ray diffraction (XRD) analysis of the as-received and postdeformed samples, which indicate γ -iron peaks only. Due to the small dimensions of the specimen, the XRD signal from the postcompression sample is significantly less than the other signals. The intensity is lower by an order of magnitude but all peaks are present. The relative magnitudes of the peaks also change. For example, in the posttension XRD scan, the (200) peak is absent. Further, while pole figure analysis (not shown) indicates that the texture of the steel is rather mild, these changes imply that the texture evolves during deformation.

SecoSal300 - X-Ray Diffraction Scan
As-Received, Post-Tension, and Post-Dynamic Compression

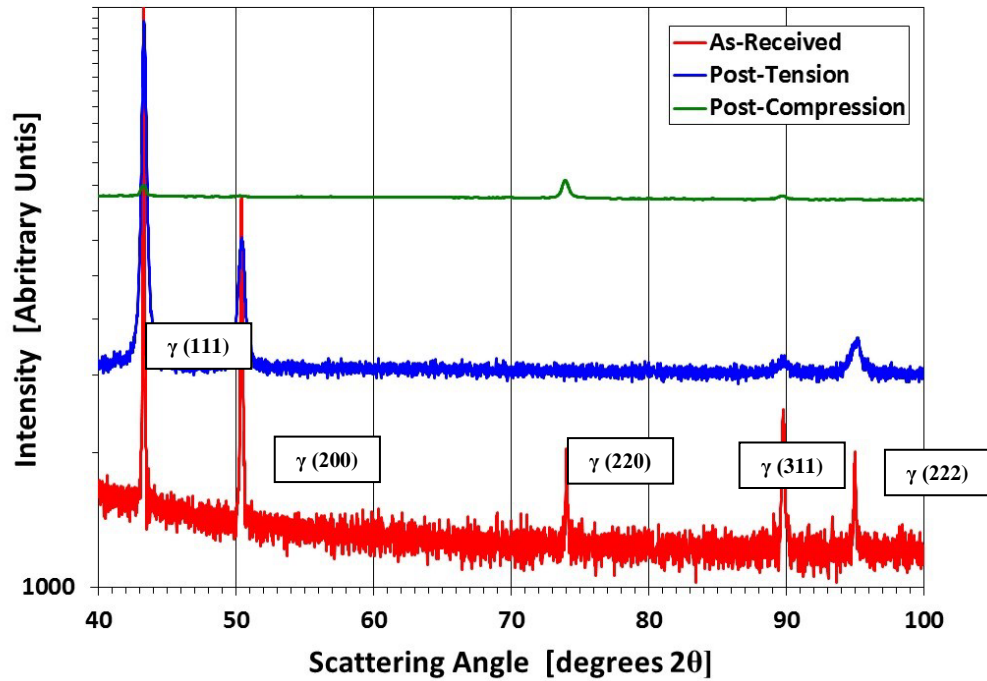


Fig. 5 XRD scan of the SecoSal300 steel. The data reveal the Bragg peaks due to γ -Fe only. The scans were plotted on a logarithmic scale and the individual scans were offset for clarity.

The quasi-static mechanical properties of the SecoSal300 steel are summarized in Fig. 6. Specifically, the data show that the material is highly isotropic as the results in the rolling, transverse, and normal directions are virtually identical. Furthermore, the material tested at quasi-static rates in tension and compression reveals almost no tension-compression asymmetry. The stress-strain curves in compression were stopped at a strain of 0.30 as the test was terminated at that point. The quasi-static yield point is around 600 MPa with a tensile strength of about 1600 MPa.

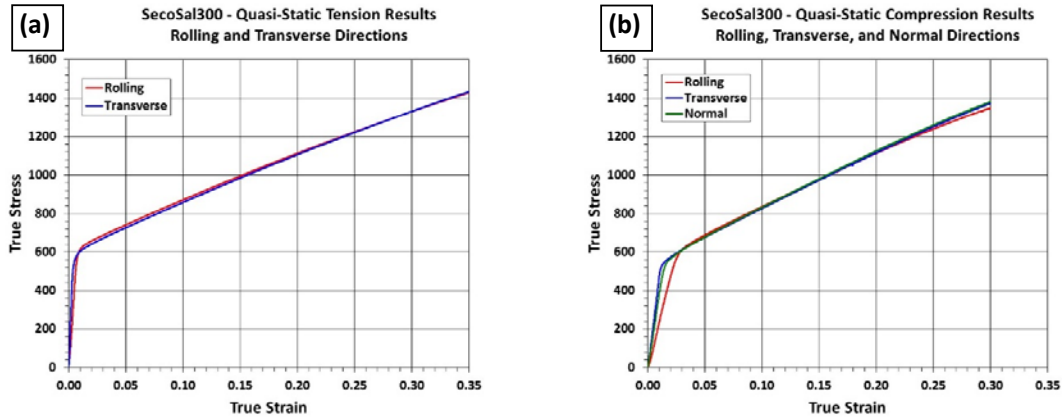


Fig. 6 Quasi-static true stress-true strain curves for the SecoSal300 Salzgitter steel: a) tension and b) compression data for all orientations relative to the rolling direction. Despite the rolling, the response of the material is isotropic.

Similar to the quasi-static results, the dynamic stress-strain curves show a very uniform and isotropic material response (Fig. 7). However, there is a significant increase in the dynamic yield strength to about 1000 MPa. The dynamic flow stress is not as high, as it is only about 1400 MPa at a compressive strain of about 0.25. Closer inspection of the quasi-static tensile and compressive stress-strain curves show that the initially very high work-hardening rate decreases rapidly after yielding, followed by a steady linear decrease up to strains of 0.30 and beyond. The strain-hardening exponent was determined to be about 0.35. The strain-rate sensitivity was determined to be 0.075.

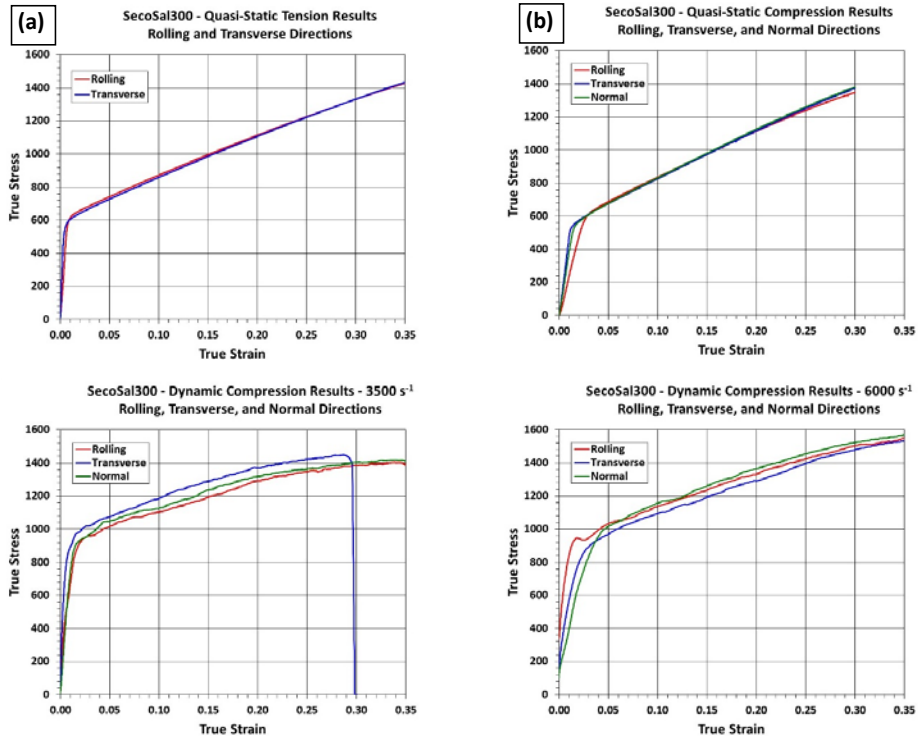


Fig. 7 Dynamic compressive true stress-true strain curves for the SecoSal300 Salzgitter steel: a) response at 3500 s⁻¹ and b) response at 6000 s⁻¹. Both these data and a comparison with the quasi-static compression data show that the material has a very strong strain-hardening response. Again, note the isotropy of the material.

SEM observations of the samples after dynamic loading show the uniform and bulk deformation without any type of shear localization in the steel (Fig. 8).

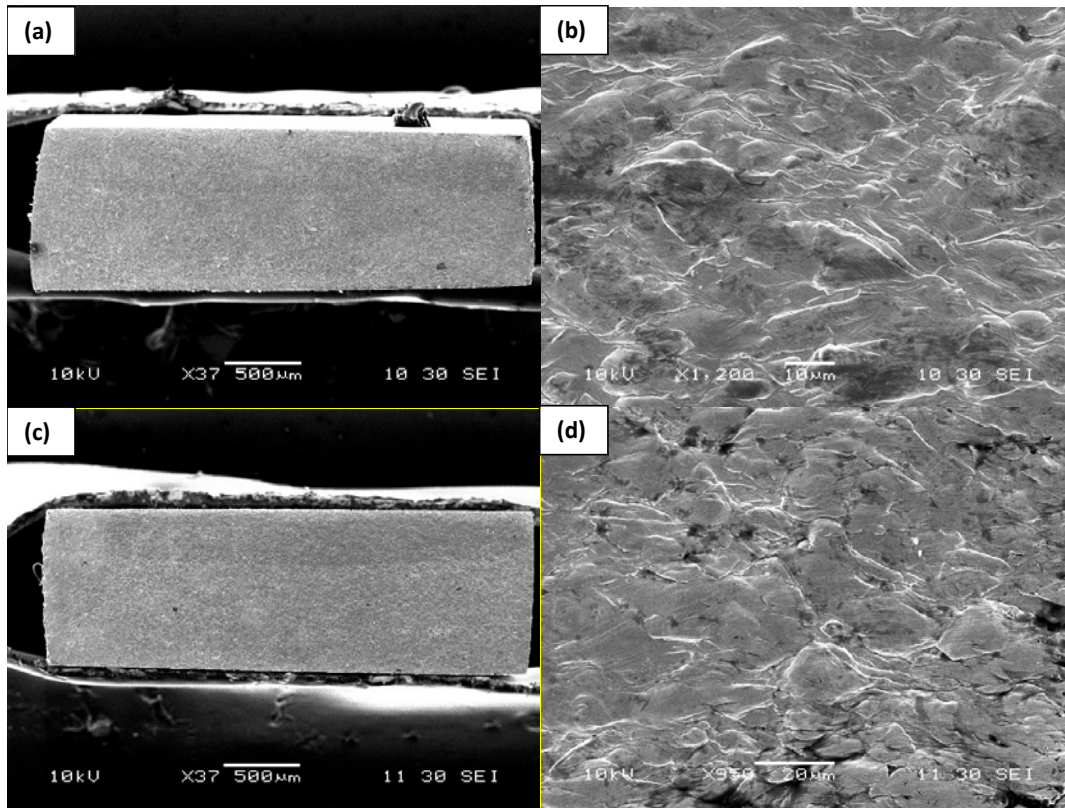


Fig. 8 Postmortem SEM of the dynamic compression samples, tested at 6000 s^{-1} . Images show a) macro and b) microscale views of the specimen loaded in the transverse direction and c) macro- and d) microscale views of the specimen loaded in the rolling direction.

TEM observations of the tested material after quasi-static tension and dynamic compression revealed that the steel deforms by deformation twinning. The BF and SADPs in Fig. 9 illustrate nicely the presence of the nanoscale twins induced during deformation.

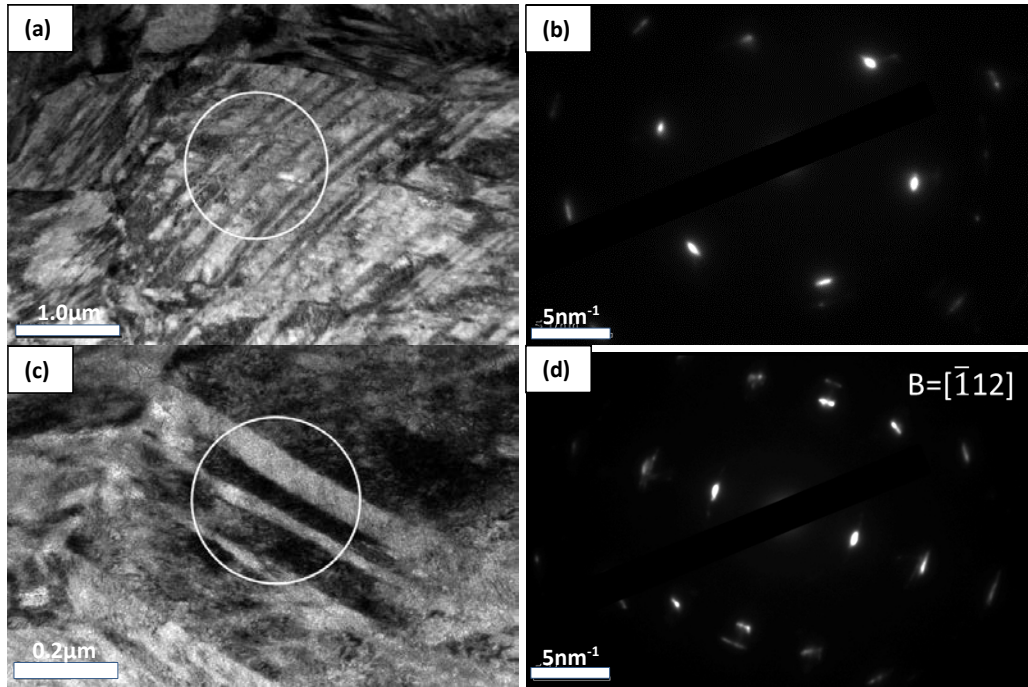


Fig. 9 TEM micrographs of the SecoSal300 Salzgitter steel after tension testing: a) typical BF image with nanoscale twins, b) corresponding SADP, c) another region showing the presence of twins, and d) corresponding SADP. Note the double diffraction spots in the SADPs are attributed to twinning.

Shown in Fig. 10, postmortem examination of the quasi-static tensile sample fracture surfaces revealed a purely ductile fracture in this steel. The macrographs are indicative of some necking. Further examination of the fracture surface with SEM, shown in Fig 11, reveals a rough fracture surface with ductile dimpling on a microscopic scale.

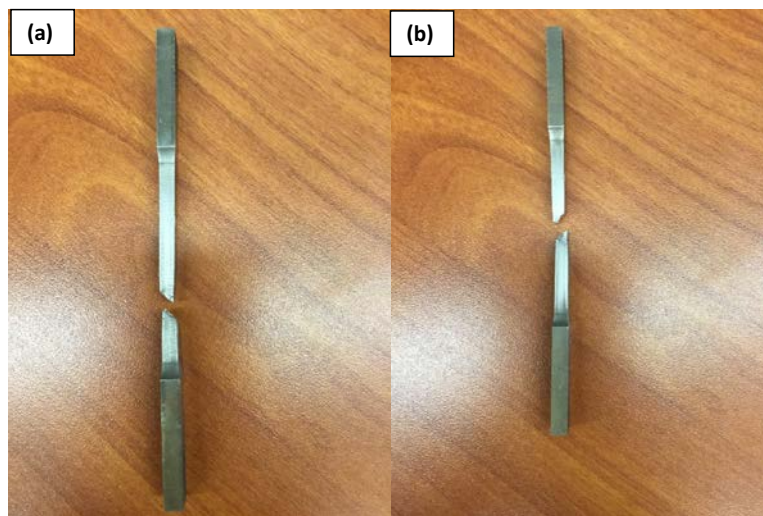


Fig. 10 Tensile test specimens after failure, rolling direction a) and transverse b) direction, respectively.

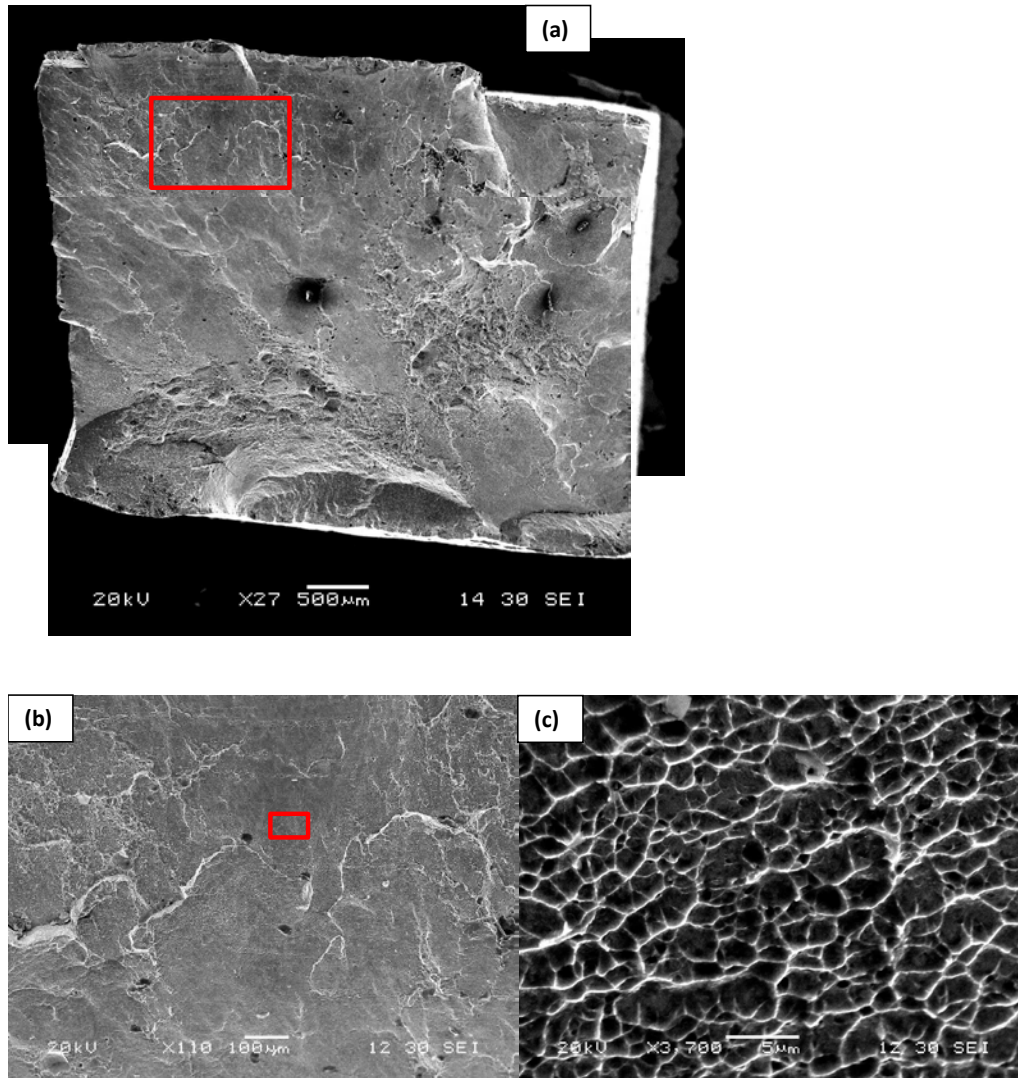


Fig. 11 SEM of the fracture surface at increasing magnifications. Composite image in a), and higher magnifications revealing the ductile nature of the failure in b) and c), respectively.

4.2 Ballistic Testing

Ballistic testing was performed on a 5-mm thick RHA plate to serve as a baseline and the Salzgitter steel using a 0.30-cal. M2 ball projectile and a 0.30-cal. FSP. Dimensions for both projectiles are shown in Figs. 12 and 13. The M2 ball projectile has a nominal mass of 9.72 g. This projectile has a sharp ogive nose, a lead core, and a gilding metal jacket. The FSP has a nominal mass of 2.85 g and a hardness of 30 Rockwell C. As such, it is expected that the response of the steel target would be different to these 2 threat types. Specifically, shear failure was expected for the ball projectile, whereas plugging failure was expected for the FSP.

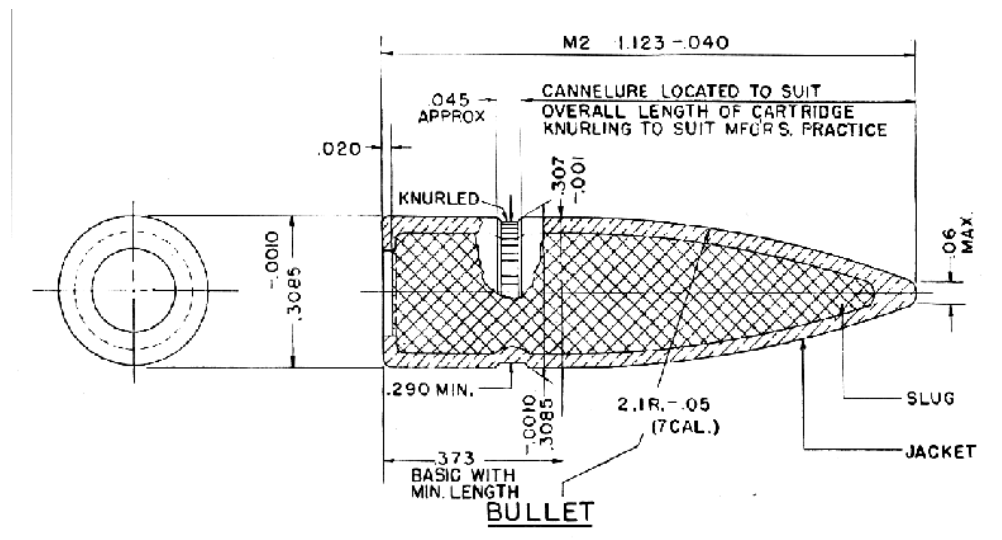


Fig. 12 Schematic of the 0.30-cal. M2 ball projectile¹⁶

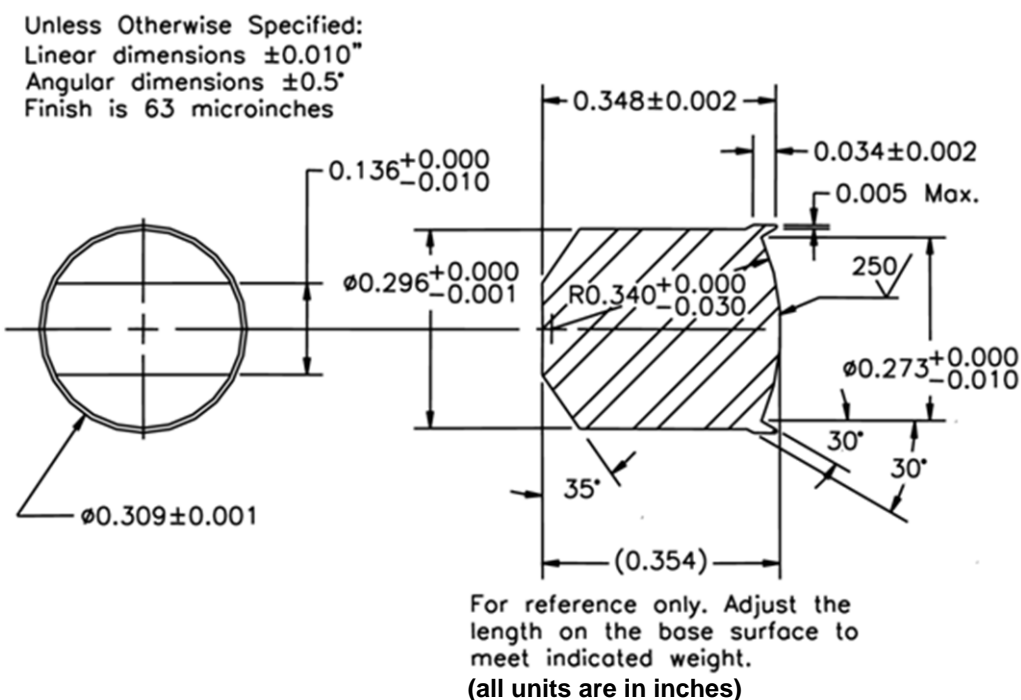


Fig. 13 Schematic of the 0.30-cal. FSP¹⁷

The target plate was positioned at a 30° obliquity to the projectile's path of flight at impact for the M2 ball projectile. The target plate was positioned normal (0° obliquity) to the projectile's path of flight at impact for the 0.30-cal. FSP projectile. The M2 ball projectile and target obliquity was in accordance with the ballistic test requirements of US Department of Defense MIL-A-12560K for 5-mm steel.³ Each plate was tested to determine the V_{50} ballistic limit values and notable differences,

if any, in the material's failure characteristics. The V_{50} ballistic limit and sample standard deviation were calculated in accordance with the US Department of Defense MIL-STD-662F.¹⁸

The RHA plates were cut to a 305- × 305-mm square target dimension for testing. The average thickness of each RHA plate was measured. The hardness of each plate was measured on the Brinell scale. Ballistic test results are summarized in Table 2. The detailed ballistic data are provided in the Appendix.

Table 2 Ballistic results of the RHA and Salzgitter steel plates vs. the 0.30-cal. M2 ball projectile and the 0.30-cal. FSP

Plate details			0.30-cal. M2 ball at 30° obliquity		0.30-cal. FSP at 0° obliquity	
Shot number (plate ID)	Thickness (mm)	Hardness (HBN)	V_{50} (m/s)	Standard deviation (m/s)	V_{50} (m/s)	Standard deviation (m/s)
13354-13363 (RHA)	4.947	351	694	9
13345-13353 (Salzgitter)	5.004	248	737	12
13372-13385 (RHA)	4.947	351	803	15
13366-13371 (Salzgitter)	5.004	248	614	4

Postballistic testing photographs of the front and back surfaces of the Salzgitter steel and RHA plates are shown in Figs. 14–17. The numerical values written on the plates are shot identification numbers.



Fig. 14 Postballistic front and back side photographs of the 5.004-mm Salzgitter steel plate vs. the 0.30-cal. M2 ball projectile. Note the bulging of the back face for the penetrators that did not perforate the plate.



Fig. 15 Postballistic front and back side photographs of the 4.947-mm RHA plate vs. the 0.30-cal. M2 ball projectile. Note the lack of bulging for the penetrators that did not perforate the plate.



Fig. 16 Postballistic front and back side photographs of the 5.004-mm Salzgitter steel plate vs. the 0.30-cal. FSP



Fig. 17 Postballistic front and back side photographs of the 4.947-mm RHA plate vs. the 0.30-cal. FSP

At impact and during penetration, the prevalent failure mechanism for the M2 ball projectile is expected to be bulk deformation of the plate material as it is pushed to the side by the advancing projectile, followed by adiabatic shear localization along the highly strained regions once the local shear strength is exceeded. Concurrent with the deformation of the plate, the erosion of the penetrator can be significant. The lower hardness and higher ductility of the Salzgitter plate decelerated the projectile and dissipated the projectile's energy through bulging. That is, this bulk deformation process or bulging was a more efficient energy dissipation and absorption mechanism to stop the penetrator, which, in turn, delayed the eventual adiabatic shear failure of the steel. In contrast, the postballistic photographs revealed that the higher hardness RHA did not bulge as much, and thus did not delay the onset of the inevitable adiabatic shear failure process during penetration. There were no penetrators captured for either steel plate type because the soft lead

core was not able to perforate the plates. Overall, the Salzgitter steel plate performed slightly better and exhibited a 6% improvement in ballistic penetration resistance over the RHA plates against the M2 ball projectile.

Unlike the M2 ball projectile, the steel FSP is a circular cylinder with a blunter, chamfered nose. As such, due to the wider surface contact area at impact, its deformation behavior is expected to be different. That is, lateral bulk deformation cannot occur as readily and, instead, under the influence of the increasing stress concentration caused by the edge of the projectile, shear plugging is more likely to occur. From the onset, for the Salzgitter steel plate, the projectile decelerated and, its energy was dissipated through bulging; consequently, the eventual plugging failure was somewhat delayed. However, the postballistic photographs revealed that the harder RHA behaved differently. Though, the plate somewhat bulged before plugging. Nevertheless, it was the much higher hardness of the RHA compared to the softer FSP that was the critical material property in its ability to decelerate this projectile more effectively. As such, the RHA plates performed significantly better and exhibited a 24% improvement in ballistic penetration resistance over the Salzgitter steel plate against the FSP.

It would have been interesting to study the erosion behavior of the various projectiles embedded in these steel plates; however, that was outside of the scope of this study. Nevertheless, these results indicate that the projectile core hardness and overall projectile nose shape are both equally important during penetration into steel.¹⁹ The difference between the ballistic limit of the 2 steels against the soft lead core M2 ball projectile was 43 m/s. However, the corresponding difference between the ballistic limits of these 2 steels against the FSP that has a mild hardness was much greater, 189 m/s. For the ball projectile, it is the ductility or the ability of the steel that allows lateral deformation as an operational energy dissipation mechanism. Based on the V_{50} results, this energy dissipation mechanism was slightly more effective in the Salzgitter steel. In contrast, for the FSP, it is the relative hardness (or yield strength) of the steel plate, compared with that of the projectile, that controls the deceleration process. Because the RHA is harder than the FSP and the Salzgitter steel is softer than the FSP, the RHA is more effective.

Our tests reveal that a single material property (i.e., ductility versus hardness) can be optimized to defeat a single type of threat. However, a better design approach would be to consider the tradeoffs between such properties, which, in turn, will ultimately determine the effective resistance to both type of threats. In this comparative study, with all other factors being essentially the same, because of the higher hardness of the RHA, its overall performance was found to be better.

5. Summary and Conclusions

Our metallurgical analyses confirmed the data provided by Salzgitter. Ballistic evaluations against the 2 threats produced mixed results. Specifically, the Salzgitter steel plate provided only a 6% improvement in ballistic penetration resistance over the harder RHA plates against the M2 ball projectile. In contrast, the RHA plates exhibited a 24% improvement in ballistic penetration resistance over the Salzgitter steel plate against the FSP. Both of these results were consistent with the German evaluation. It is believed that the lower hardness of the Salzgitter steel plate is able to arrest the M2 ball because of its lead core. However, the harder steel FSP required a harder impact surface to provide an improved penetration resistance, but with its lower hardness, the Salzgitter steel could not satisfy this condition. As such, the RHA showed a better ability to mitigate the challenges of both project types than the Salzgitter steel plate.

Overall, the completion of this project provided an increased understanding of how steel composition affects V_{50} limit velocities for a range of threats. Furthermore, our comparative study has shown that with its properties, the Salzgitter steel, intended for commercial applications, does not have the properties required by armor applications. In other words, the critical and optimized property parameters of RHA (i.e., the characteristic tradeoff between strength and ductility) render it to be a better armor material than the Salzgitter steel. However, where slight reductions in weight is a benefit, the latter may meet certain applications. However, again to reiterate, this grade of steel is still at an early developmental stage as there are serious thickness limitations in its fabrication.

6. References

1. Hadfield R, Burnham TH. Special steels. 2nd ed. New York (NY): The Pitman Press; 1933. p. 100.
2. Owen WS, Grujicic M. Strain aging of austenitic Hadfield manganese steel. *Acta Materialia*. 1998;47:111–126.
3. MIL-A-12560K. Detail specification: armor plate, steel, wrought, homogeneous (for use in combat-vehicles and for ammunition testing. Aberdeen Proving Ground (MD): Army Research Laboratory (US); 2013 Dec 7.
4. Montgomery JS, Wells MGH, Roopchand B, Ogilvy JW. Low-cost titanium armors for combat vehicles. *Journal of Metals*, 1997;49(5):45-47.
5. Burkins MS, Gooch W. US Army Research Laboratory, Aberdeen Proving Ground, MD. Personal communication, 2004 Feb.
6. Commission on Engineering and Technical Systems. Reducing the logistics burden for the army after next: doing more with less. Appendix D. Washington (DC): National Research Council; 1999.
7. Han SH, Shin BC, Lee W, Choi JH. Fatigue crack propagation life of partially penetrated butt welds in steel structures. Paper presented at the CM9; 25–29 May 2003; Palexpo Congress Center, Geneva, Switzerland.
8. Jones TL. The effects of heat treatment on the ballistic protection of rolled homogeneous armor (RHA). Aberdeen Proving Ground (MD): Army Research Laboratory (US); 2004 Dec. Report No.: ARL-TR-3379.
9. ASTM E1019-11. Standard test methods for determination of carbon, sulfur, nitrogen, and oxygen in steel, iron, nickel, and cobalt alloys by various combustion and fusion techniques. West Conshohocken (PA): ASTM International; 2011.
10. ASTM E1447-09 (2016). Standard test method for determination of hydrogen in titanium and titanium alloys by inert gas fusion thermal conductivity/infrared detection method. West Conshohocken (PA): ASTM International; 2016.
11. ASTM E1097-12. Standard guide for determination of various elements by direct current plasma atomic emission spectrometry. West Conshohocken (PA): ASTM International; 2012.

12. Hong S, Shin SY, Kim HS, Lee S, Kim SK, Chin KG, Kim NJ. Metallurgical and Materials Transactions A-Physical Metallurgy and Materials Science. 2013;44A:776–786.
13. ASTM E8/E8M-16a. Standard test methods for tension testing of metallic materials. West Conshohocken (PA): ASTM International; 2016.
14. Follansbee PS. The Hopkinson bar. metals handbook. 9th ed. Mechanical Testing, vol. 8, Metals Park (OH): American Society of Materials; 1985. p. 198–217.
15. Gray GT. High strain rate testing of materials: the split Hopkinson pressure bar. Methods in Materials Research. New York (NY): John Wiley Press; 2000.
16. M2 ball bullet, part no. 6171958 drawing. Philadelphia (PA): Army Frankford Arsenal (US); 1940 Sep.
17. MIL-P-46593A (ORD). Military specification: projectile, calibers, .22, .30, .50 and 20 mm fragment simulating. Picatinny Arsenal (NJ): US Army; 1962.
18. MIL-STD-622F. Military standard: V50 ballistic test for armor. Aberdeen Proving Ground (MD): US Department of Defense; 1997.
19. Jones TL. A study on the influence of projectile core hardness on the ballistic penetration into ceramic armor. Aberdeen Proving Ground (MD): Army Research Laboratory (US); 2014 Sep. Report No.: ARL-TR-7112.

Appendix. Ballistic Test Data

This appendix appears in its original form, without editorial change.

Approved for public release; distribution is unlimited.

0.30-cal M2 Ball Projectile – RHA Steel

Target:	RHA Steel				Date:	5-May-2016		
Plate #:	N/A				Test Site:	EF-108		
Lot #:	N/A							
Average Thickness:	0.195 inches			4.947 mm				
Hardness:	351 BHN							
Target Obliquity at Impact:	30°							
Projectile:	0.30 cal M2 Ball			Lot #: LC13943				
Setup:	Steel - Air (6") - AA2024 (0.020")							
Velocity Measurement:	Striking X-rays							
Low CP:	2258	ft/s		688	m/s			
High PP:	2291	ft/s		698	m/s			
V50:	2278	ft/s		694	m/s	# Shots:	4	
Std. Dev.:	28	ft/s		9	m/s	Spread:	59 ft/s	18 m/s
ZMR:	33	ft/s		10	m/s			
Shot #	Striking Velocity [ft/s]	Striking Velocity [m/s]	Pitch [degrees]	Yaw [degrees]	Gamma [degrees]	Results [PP/CP]	Used for V50	Comments
13354	2635	803			0.18	CP	No	
13355	2529	771			0.15	CP	No	
13356	2291	698			0.50	PP	Yes	
13357	2312	705			0.61	CP	No	
13358	2379	725			0.78	CP	No	
13359	2379	725			0.52	CP	No	
13360	2343	714			0.45	CP	No	
13361	2258	688			0.65	CP	Yes	
13362	2311	704			0.45	CP	Yes	
13363	2252	686			0.33	PP	Yes	

0.30-cal M2 Ball Projectile – German Salzgitter Steel

Target:	German Salzgitter Steel				Date:	May-4-2016		
Plate #:	N/A				Test Site:	EF-108		
Lot #:	N/A							
Average Thickness:	0.197 inches		5.004 mm					
Hardness:	248 BHN							
Target Obliquity at Impact:	30°							
Projectile:	0.30 cal M2 Ball	Lot #:	LC13943					
Setup:	Steel - Air (6") - AA2024 (0.020")							
Velocity Measurement:	Striking X-rays							
Low CP:	2447 ft/s		746 m/s					
High PP:	2382 ft/s		726 m/s					
V50:	2417 ft/s		737 m/s		# Shots:	6		
Std. Dev.:	40 ft/s		12 m/s		Spread:	83 ft/s		25 m/s
ZMR:	0 ft/s		0 m/s					
Shot #	Striking Velocity [ft/s]	Striking Velocity [m/s]	Pitch [degrees]	Yaw [degrees]	Gamma [degrees]	Results [PP/CP]	Used for V50	Comments
13345	2233	681			0.62	PP	No	
13346	2382	726			0.26	PP	Yes	
13347	2514	766			0.36	CP	No	
13348	2360	719			0.77	PP	No	
13349	2449	746			0.34	CP	Yes	
13350	2447	746			0.59	CP	Yes	
13351	2462	750			0.58	CP	Yes	
13352	2381	726			0.64	PP	Yes	
13353	2379	725			0.41	PP	Yes	

0.30-cal FSP – RHA Steel

Target:	RHA Steel			Date:	May 12, 2016			
Plate #:	N/A			Test Site:	EF-108			
Lot #:	N/A							
Average Thickness:	0.197 inches		5.004 mm					
Hardness:	351 BHN							
Target Obliquity at Impact:	0°							
Projectile:	0.30 cal FSP	Lot #:						
Setup:	Steel - Air (6") - AA2024 (0.020")							
Velocity Measurement:	Striking X-rays - For Shot #s 13375-13376; Chronograph for Shot #s 13372-13374 and Shot #s 13377-13385							
Chronograph Correction:	For Shot #s 13372-13374: 0.962472406; For Shot #s 13377-13385: 0.961038961							
Low CP:	2615 ft/s		797 m/s					
High PP:	2672 ft/s		814 m/s					
V50:	2634 ft/s		803 m/s	# Shots:	10			
Std. Dev.:	48 ft/s		15 m/s	Spread:	138 ft/s		42 m/s	
ZMR:	57 ft/s		17 m/s					
Shot #	Striking Velocity [ft/s]	Striking Velocity [m/s]	Pitch [degrees]	Yaw [degrees]	Gamma [degrees]	Results [PP/CP]	Used for V50	Comments
13372	1988	606				PP	No	
13373	2187	667				PP	No	
13374	2315	706				PP	No	
13375	2535	773			0.44	PP	No	
13376	2664	812			0.51	CP	Yes	
13377	2615	797				CP	Yes	Used new correction factor for chronograph
13378	2579	786				PP	Yes	
13379	2568	783				PP	Yes	
13380	2678	816				CP	Yes	
13381	2585	788				PP	Yes	
13382	2672	814				PP	Yes	
13383	2706	825				CP	Yes	
13384	2660	811				CP	Yes	
13385	2611	796				PP	Yes	

0.30-cal FSP – German Salzgitter Steel

Target:	German Salzgitter Steel			Date:	May 11, 2016			
Plate #:	N/A			Test Site:	EF-108			
Lot #:	N/A							
Average Thickness:	0.197 inches		5.004 mm					
Hardness:	248 BHN							
Target Obliquity at Impact:	0°							
Projectile:	0.30 cal FSP	Lot #:						
Setup:	Steel - Air (6") - AA2024 (0.020")							
Velocity Measurement:	Striking X-rays - For Shot # 13366; Chronograph for Shot #s 13367-13371							
Chronograph Correction:	For Shot #s 13367-13371: 0.962472406							
Low CP:	2025 ft/s		617 m/s					
High PP:	2006 ft/s		611 m/s					
V50:	2014 ft/s		614 m/s	# Shots:	4			
Std. Dev.:	14 ft/s		4 m/s	Spread:	29 ft/s			9 m/s
ZMR:	0 ft/s		0 m/s					
Shot #	Striking Velocity [ft/s]	Striking Velocity [m/s]	Pitch [degrees]	Yaw [degrees]	Gamma [degrees]	Results [PP/CP]	Used for V50	Comments
13366	2180	664			0.55	CP	No	
13367	2006	611				PP	Yes	Used new correction factor for chronograph
13368	2094	638				CP	No	
13369	2025	617				CP	Yes	
13370	2027	618				CP	Yes	
13371	1998	609				PP	Yes	

INTENTIONALLY LEFT BLANK.

List of Symbols, Abbreviations, and Acronyms

ARL	US Army Research Laboratory
BCC	body-centered cubic
BF	bright field
EDM	electric discharge machining
FCC	face-centered cubic
FSP	fragment-simulating projectile
RHA	rolled homogeneous armor
SADP	selected area diffraction pattern
SEM	scanning electron microscopy
SFE	stacking fault energy
TEM	transmission electron microscopy
TRIP	transformation-induced plasticity
TWIP	twinning-induced plasticity
XRD	X-ray diffraction

1 DEFENSE TECHNICAL
(PDF) INFORMATION CTR
DTIC OCA

2 DIRECTOR
(PDF) US ARMY RESEARCH LAB
RDRL CIO L
IMAL HRA MAIL & RECORDS
MGMT

1 GOVT PRINTG OFC
(PDF) A MALHOTRA

18 DIR USARL
(PDF) RDRL WMM
M VANLANDINGHAM
R DOWDING
RDRL WMM F
J CHINELLA
L DOUGHERTY
S GREND AHL
V HAMMOND
E HORWATH
L KECSKES
K LIMMER
T SANO
M TSCHOPP
RDRL WML
N TRIVEDI
RDRL WML H
L MAGNESS
B SCHUSTER
RDRL WMP
D LYON
RDRL WMP E
T JONES
M BURKINS
P SWOBODA